Scale dependence of energy transfer in turbulent plasma

Yan Yang [1,2]★ Minping Wan,[1]★ William H. Matthaeus,[3] Luca Sorriso-Valvo,[4,5] Tulasi N. Parashar,[3] Quanming Lu,[2] Yipeng Shi[6] and Shiyi Chen[1]

[1]*Southern University of Science and Technology, Shenzhen, Guangdong 518055, China*
[2]*University of Science and Technology of China, Hefei, Anhui 230026, China*
[3]*University of Delaware, Newark, DE 19716, USA*
[4]*Nanotec/CNR, Sede di Cosenza, Ponte P. Bucci, Cubo 31C, 87036 Rende, Italy*
[5]*Departmento de Fisica, Escuela Polotecnica Nacional, Quito 170517, Ecuador*
[6]*Peking University, Beijing 100871, China*

ABSTRACT

In the context of space and astrophysical plasma turbulence and particle heating, several vocabularies emerge for estimating turbulent energy dissipation rate, including Kolmogorov–Yaglom third-order law and, in its various forms, $\boldsymbol{j} \cdot \boldsymbol{E}$ (work done by the electromagnetic field on particles), and $-(\boldsymbol{P} \cdot \nabla) \cdot \boldsymbol{u}$ (pressure–strain interaction), to name a couple. It is now understood that these energy transfer channels, to some extent, are correlated with coherent structures. In particular, we find that different energy dissipation proxies, although not pointwise correlated, are concentrated in proximity to each other, for which they decorrelate in a few ion inertial scales. However, the energy dissipation proxies dominate at different scales. For example, there is an inertial range over which the third-order law is meaningful. Contributions from scale bands stemming from scale-dependent spatial filtering show that the energy exchange through $\boldsymbol{j} \cdot \boldsymbol{E}$ mainly results from large scales, while the energy conversion from fluid flow to internal through $-(\boldsymbol{P} \cdot \nabla) \cdot \boldsymbol{u}$ dominates at small scales.

Key words: MHD – plasmas – turbulence – solar wind.

1 INTRODUCTION

Energy dissipation mechanism for weakly collisional or collisionless plasma is of principal importance for addressing long-standing puzzles like the acceleration of energetic particles, and related questions that arise in space and astrophysical applications such as the solar wind. Depending on the plasma conditions, different dissipative mechanisms like wave–particle interactions (Hollweg 1986; Hollweg & Isenberg 2002; Gary & Saito 2003; Markovskii et al. 2006; Gary, Saito & Li 2008; Howes et al. 2008; He et al. 2015a,b) and heating by coherent structures and reconnection (Dmitruk, Matthaeus & Seenu 2004; Retinò et al. 2007; Sundkvist et al. 2007; Parashar et al. 2011; Perri et al. 2012; TenBarge & Howes 2013; He et al. 2018), might be dominant at kinetic scales. This question is inherently related to an open debate as to whether the fluctuations in the solar wind are interacting waves, nonlinearly evolving turbulence, or their mutual competition, each having its adherents (Goldreich & Sridhar 1995; Bale et al. 2005; Howes et al. 2008, 2011; Saito et al. 2008; Schekochihin et al. 2008; Sahraoui et al. 2009, 2010; Narita et al. 2011; Smith, Vasquez & Hollweg 2012). Here we focus on well-defined quantitative parameters that describe

collisionless dissipation without being sidetracked by these controversies.

While at small scales kinetic processes must be considered, the magnetohydrodynamic (MHD) model remains a credible approximation for a kinetic plasma at scales large enough to be well separated from kinetic effects. Therefore instead of studying specific mechanisms at kinetic scales, one can invoke classical turbulence theory at MHD scales. A standard turbulence scenario inherited from hydrodynamics displays an energy cascade process over the MHD inertial range. In MHD, the energy cascade within the inertial range satisfies the Politano–Pouquet law (Politano & Pouquet 1998) that describes the scaling law of the mixed third-order moments of Elsasser fields increments. Under suitable assumptions (i.e. isotropy, homogeneity, time stationarity, and incompressibility), the third-order law follows a linear scaling relation with scale separation and is proportional to mean energy dissipation rate. The Politano–Pouquet law has been examined in the solar wind (Sorriso-Valvo et al. 2007; MacBride & Smith 2008; Marino et al. 2008; Stawarz et al. 2009; Coburn et al. 2015; Bandyopadhyay et al. 2018a) and in numerical simulations (Sorriso-Valvo et al. 2002, 2018a). A number of studies have also taken into account corrections from anisotropy (Podesta 2008; Wan et al. 2009, 2010; Osman et al. 2011; Stawarz et al. 2011), compressibility (Carbone et al. 2009; Kritsuk et al. 2009; Forman, Smith & Vasquez 2010;

★ E-mail: yanyangpku@gmail.com (YY); wanmp@sustc.edu.cn (MW)

Sorriso-Valvo et al. 2010; Marino et al. 2011; Banerjee & Galtier 2013; Banerjee et al. 2016; Hadid, Sahraoui & Galtier 2017), solar wind shear (Wan et al. 2009, 2010) and expansion (Gogoberidze, Perri & Carbone 2013; Hellinger et al. 2013) and Hall effect (Galtier 2008; Andrés, Galtier & Sahraoui 2018; Hellinger et al. 2018), to name a few. More recently, Bandyopadhyay et al. (2018b) found that the standard Kolmogorov cascade may be operative at a diminished intensity even in the kinetic scales, as an ingredient of a complex cascade accommodating kinetic effects. We avoid all such complications here in an effort to elucidate possible correlations amongst several basic estimations of energy dissipation rate (energy dissipation proxies).

'Dissipation' in this paper simply refers to the increase in internal energy of distribution functions. This increase in internal energy is eventually 'thermalized' by infrequent collisions but this irreversibility is not our focus here. The work done by the electromagnetic field on particles, $\boldsymbol{j} \cdot \boldsymbol{E}$ (Wan et al. 2012, 2015; Osman et al. 2015; Fu et al. 2017; Yao et al. 2017; Chasapis et al. 2018a; Ergun et al. 2018; Howes, McCubbin & Klein 2018), although not strictly irreversible dissipation, is the necessary energy supply from electromagnetic fields that ultimately goes into the internal energy reservoir. It is therefore customary to deem $\boldsymbol{j} \cdot \boldsymbol{E}$ as a dissipation proxy, which is highly localized in association with current sheets (Wan et al. 2012, 2015; Osman et al. 2015; Chasapis et al. 2018a). A basic question, however, is what fraction of the electromagnetic energy released through $\boldsymbol{j} \cdot \boldsymbol{E}$ ends up as ion and electron random motion as opposed to fluid flow. To this end, Yang et al. (2017a,c) proposed recently that the interaction between pressure tensor and strain tensor, $-(\boldsymbol{P} \cdot \nabla) \cdot \boldsymbol{u}$, is responsible for the generation of plasma internal energy. This idea can be traced back to early works by Braginskii (1965), which is generalized into the kinetic realm of collisionless systems by Del Sarto et al. (Del Sarto, Pegoraro & Califano 2016; Del Sarto & Pegoraro 2017) as well. More recently, there is growing evidence that elucidates the role of pressure–strain interaction using numerical simulations (Sitnov et al. 2018) and observations (Chasapis et al. 2018b).

The work done so far has not specifically emphasized the associations and differences that exist among these dissipation proxies, yet simulations and observations indicate that each of them plays an important role in the heating process. Here we seek to describe their correlations. To take it further, they might differ from each other in many ways as well. We adopt a narrow tack here, inquiring at what scales the different proxies dominate, thus providing more detail concerning energy transfer from macroscopic fluid scales to kinetic scales.

2 SIMULATION DETAILS

Here we employ a fully kinetic simulation by P3D (Zeiler et al. 2002) in 2.5D geometry (three components of dependent field vectors and a two-dimensional spatial grid). Number density is normalized to a reference number density n_r (= 1 in this simulation), mass to proton mass m_i (= 1 in this simulation), charge to proton charge q_i, and magnetic field to a reference B_r (= 1 in this run). Length is normalized to the ion inertial length d_i, time to the ion cyclotron time Ω_i^{-1}, velocity to the reference Alfvén speed $v_{Ar} = B_r/(4\pi m_i n_r)^{1/2}$, and temperature to $T_r = m_i v_{Ar}^2$. The simulation was performed in a periodic domain, whose size is $L \simeq 150 d_i$, with 4096^2 grid points and 3200 particles of each species per cell ($\sim 107 \times 10^9$ total particles). The ion to electron mass ratio is $m_i/m_e = 25$, and the speed of light in the simulation is $c = 15 v_{Ar}$. Although small mass ratio and low speed of light might introduce some unrealistic effects, they are
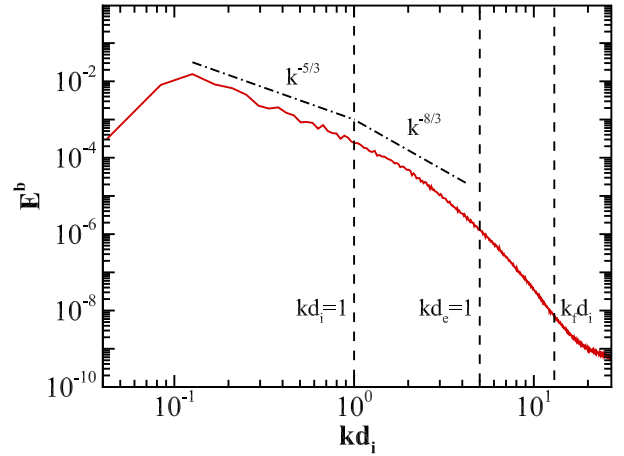

Figure 1. Omnidirectional energy spectrum of magnetic fluctuations (prior to filtering). Power laws are shown for reference. Vertical lines are drawn at wavenumbers corresponding to ion inertial scale, to electron inertial scale, and at the filtering scale, as explained in the text.

necessary compromises to attain a large simulated system size L/d_i, and a reasonably large particle number per cell, which also running for long dynamical times. This run is a decaying initial value problem, starting with uniform density ($n_0 = 1.0$) and temperature of ions and electrons ($T_0 = 0.3$). The uniform magnetic field is $B_0 = 1.0$ directed out of the plane. This simulation is a part of a set of simulations to study kinetic plasma turbulence as a function of plasma β (Parashar, Matthaeus & Shay 2018).

We analyse statistics using a snapshot near the time of maximum root mean square (r.m.s.) electric current density (i.e., $t\Omega_i = 99.0$). Fig. 1 shows the omnidirectional energy spectrum of magnetic fluctuations, where $k^{-5/3}$ and $k^{-8/3}$ power laws are shown for reference in the range $k < 1/d_i$ and $1/d_i < k < 1/d_e$, respectively. Prior to statistical analyses, we remove noise inherent in the particle-in-cell plasma algorithm through low-pass Fourier filtering of the fields at $k_f d_i \sim 13$.

3 THIRD-ORDER MOMENT ESTIMATE

In studying energy dissipation, the most satisfactory way to proceed in MHD would be to directly study the viscous and resistive dissipation functions. However, in default of an explicit expression for dissipation in collisionless plasma, it is promising to appeal to a third-order law such as (Politano & Pouquet 1998)

$$S_\parallel^\pm(r) = \langle \delta z_\parallel^\mp \delta z_i^\pm \delta z_i^\pm \rangle = -\frac{4}{d} \epsilon^\pm r \qquad (1)$$

where $\boldsymbol{z}^\pm = \boldsymbol{u} \pm \boldsymbol{b}/\sqrt{4\pi\rho}$, $\delta \boldsymbol{z}^\pm = \boldsymbol{z}^\pm(\boldsymbol{x} + \boldsymbol{r}) - \boldsymbol{z}^\pm(\boldsymbol{x})$, $\delta z_\parallel^\pm = \delta \boldsymbol{z}^\pm \cdot \boldsymbol{r}/r$, $\varepsilon^\pm$ is the mean energy transfer rate, and d is the spatial dimension ($d = 2$ in our case). Upon defining $S_\parallel = \left(S_\parallel^+ + S_\parallel^-\right)/2$, we arrive at an expression that is proportional to the total energy (kinetic and magnetic energies) transfer rate $\varepsilon = (\varepsilon^+ + \varepsilon^-)/2$ and the separation r. We investigate the validity of the aforementioned third-order law in Fig. 2, which exhibits nearly a decade of range ($\sim [2d_i, 10d_i]$) over which a linear variation with separation fits well, thus finding an approximately constant energy transfer rate across this inertial range of scales. The mean energy transfer rate evaluated within $[2d_i, 10d_i]$ range is $\epsilon = 1.87 \pm 0.20$ ($\times 10^{-4}$ $v_{Ar}^3 d_i^{-1}$). However, we should also keep in mind that the system does not necessarily realize an inertial range that terminates exactly at the ion scale, although the case at hand indeed shows a break of the
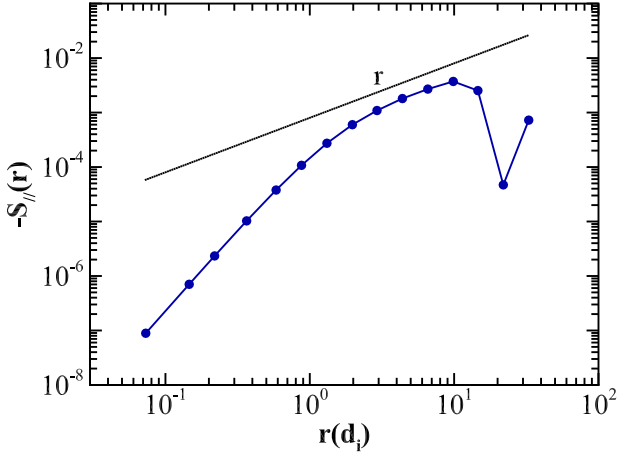
Figure 2. Mixed third-order moment of Elsasser fields increments, $S_\parallel = \left(S_\parallel^+ + S_\parallel^-\right)/2$, as a function of separation length r. A linear fit is also indicated. The mean energy transfer rate evaluated within $[2d_i, 10d_i]$ range is $\epsilon = 1.87 \pm 0.20 \, (\times 10^{-4} \, v_{Ar}^3 d_i^{-1})$.

linear law in the vicinity of the ion scale. If proceeding to smaller scales, e.g. sub-ion scales, one would prefer a dynamic law that accommodates Hall effects (Galtier 2008; Andrés et al. 2018; Bandyopadhyay et al. 2018b; Hellinger et al. 2018), a procedure that we will defer to a future study. Here we also emphasize that a compressible channel for transfer also exists (Yang et al. 2017b), but compressional effects are expected to be weak for the present quasi-incompressible turbulence simulation (as established by the density fluctuation $\delta\rho_\alpha'/\langle\rho_\alpha\rangle = \sqrt{\langle(\rho_\alpha - \langle\rho_\alpha\rangle)^2\rangle}/\langle\rho_\alpha\rangle \sim 0.07.$).

The third-order law itself is averaged over space, but is well resolved in scale. It is of interest to unravel the third-order expression, examining the contributions to the final result from each point in space. Accordingly, following Sorriso-Valvo et al. (2018a,b), we denote by $\epsilon_r^\pm$ the 'local' pseudo-energy transfer rates at the scale r,

$$\epsilon_r^\pm = -\frac{d}{4}\frac{\delta z_\parallel^\mp \delta z_i^\pm \delta z_i^\pm}{r}, \quad (2)$$

so that the 'local' total (kinetic and magnetic) energy transfer rate (LET) is computed as

$$\epsilon_r = \frac{\epsilon_r^+ + \epsilon_r^-}{2}. \quad (3)$$

The new measure, LET, is a scalar field spatially localized. However, the third-order law is only valid in a statistical (or ensemble average) sense. The LET defined in this way might be reminiscent of, but not equivalent to, the scale-to-scale energy transfer. In particular, caution is required in claiming that the LET, whose sign can be positive or negative, reveals exactly how much energy is transferred locally towards smaller or larger scales in each point of the domain. With these caveats in mind, we still believe that the LET can help to identify patches with enhanced energy transfer, as suggested in Marsch & Tu (1997) and Sorriso-Valvo et al. (2018b).

The spatial field of the LET is shown in Fig. 3, where we plot isosurfaces of the LET in a space spanned by the two spatial dimensions (x, y) and by the separation scale r. The first feature one can see is that the domain is interspersed with positive–negative alternating patches, and that moreover these patches are such that one would properly call them intermittency, since they are localized in real space and broad band in scale. The LET is signed and its point-wise magnitude could be large but significant cancellations

between opposite-signed spots lead to the global quantity dominated by the forward cascade (positive value). It is also clear that the structures are mainly sheet-like – elongated in the direction of separation length without tilt, indicating that the location of enhanced energy transfer changes very little as the scale r is varied in the inertial range.

4 DOMINANT SCALES OF ENERGY TRANSFER CHANNELS

Elementary manipulations in the full Vlasov–Maxwell system, without reliance on viscous or other closures, reveal the exchanges between electromagnetic, flow and random kinetic energy (Yang et al. 2017a,c). The first three moments of the Vlasov equation, in conjunction with the Maxwell equations, yield energy equations:

$$\partial_t \mathcal{E}_\alpha^f + \nabla \cdot \left(\mathcal{E}_\alpha^f \boldsymbol{u}_\alpha + \boldsymbol{P}_\alpha \cdot \boldsymbol{u}_\alpha\right) = (\boldsymbol{P}_\alpha \cdot \nabla) \cdot \boldsymbol{u}_\alpha + \boldsymbol{j}_\alpha \cdot \boldsymbol{E}, \quad (4)$$

$$\partial_t \mathcal{E}_\alpha^{th} + \nabla \cdot \left(\mathcal{E}_\alpha^{th} \boldsymbol{u}_\alpha + \boldsymbol{h}_\alpha\right) = -(\boldsymbol{P}_\alpha \cdot \nabla) \cdot \boldsymbol{u}_\alpha, \quad (5)$$

$$\partial_t \mathcal{E}^m + \frac{c}{4\pi}\nabla \cdot (\boldsymbol{E} \times \boldsymbol{B}) = -\boldsymbol{j} \cdot \boldsymbol{E}, \quad (6)$$

where the subscription $\alpha = e, i$ indicates the species, $\mathcal{E}_\alpha^f = \frac{1}{2}\rho_\alpha \boldsymbol{u}_\alpha^2$ is the fluid flow energy, $\mathcal{E}_\alpha^{th} = \frac{1}{2}m_\alpha \int (\boldsymbol{v} - \boldsymbol{u}_\alpha)^2 f_\alpha(\boldsymbol{x}, \boldsymbol{v}, t) \, d\boldsymbol{v}$ is the internal (thermal) energy, $\mathcal{E}^m = \frac{1}{8\pi}(\boldsymbol{B}^2 + \boldsymbol{E}^2)$ is the electromagnetic energy, $\boldsymbol{h}_\alpha$ is the heat flux vector, $\boldsymbol{j} = \sum_\alpha \boldsymbol{j}_\alpha$ is the total electric current density, and $\boldsymbol{j}_\alpha = n_\alpha q_\alpha \boldsymbol{u}_\alpha$ is the electric current density of species α. This procedure clarifies the roles of several energy transfer channels. For example, the electromagnetic work, $\boldsymbol{j} \cdot \boldsymbol{E}$, exchanges electromagnetic energy with fluid flow energy, while the pressure–strain interaction $-(\boldsymbol{P}_\alpha \cdot \nabla) \cdot \boldsymbol{u}_\alpha$ represents the conversion between fluid flow and internal energy for species α.

These energy transfer channels were studied previously in detail (Yang et al. 2017c,a), with little attempt made to describe their scales of dominance. Clearly, the plasma turbulence encompasses a vast range of scales and justification for their dominance at scales, approximate or otherwise, is crucial. A simple but essential approach to resolve fields both in space and in scales is the space-filter technique (Germano 1992), which, although pervasive in large-eddy simulations, merits more attention in the plasma turbulence community (Yang et al. 2017a; Camporeale et al. 2018). The low-pass filtered field of $\boldsymbol{a}(\boldsymbol{x})$, which only contains information at length scales $>\ell$, is defined as $\bar{\boldsymbol{a}}_\ell(\boldsymbol{x}) = \int d^3 \boldsymbol{r} G_\ell(\boldsymbol{r}) \boldsymbol{a}(\boldsymbol{x} + \boldsymbol{r})$, where ℓ is the filtering scale, $G_\ell(\boldsymbol{r}) = \ell^{-3}G(\boldsymbol{r}/\ell)$ is a filtering kernel and $G(\boldsymbol{r})$ is a normalized boxcar window function. To quantify the contribution to the field from different scales, a scale-band decomposition is introduced as

$$\boldsymbol{a}(\boldsymbol{x}) = \sum_n \boldsymbol{a}^{[n]}(\boldsymbol{x}), \quad (7)$$

where

$$\boldsymbol{a}^{[n]}(\boldsymbol{x}) = \bar{\boldsymbol{a}}_{\ell_n}(\boldsymbol{x}) - \bar{\boldsymbol{a}}_{\ell_{n+1}}(\boldsymbol{x}). \quad (8)$$

The band-filtered field $\boldsymbol{a}^{[n]}$ is therefore the fraction of the field $\boldsymbol{a}$ in band $[n]$, which contains only scales in the band (ℓ_n, ℓ_{n+1}). Here these bands are defined with a logarithmic binning $(\gamma^n \ell_0, \gamma^{n+1}\ell_0]$, where $\gamma > 1$ ($\gamma = 1.5$ is used in this work) and ℓ_0 is taken as the grid spacing of the simulation $\delta x \sim 0.0365 d_i$. Therefore, the
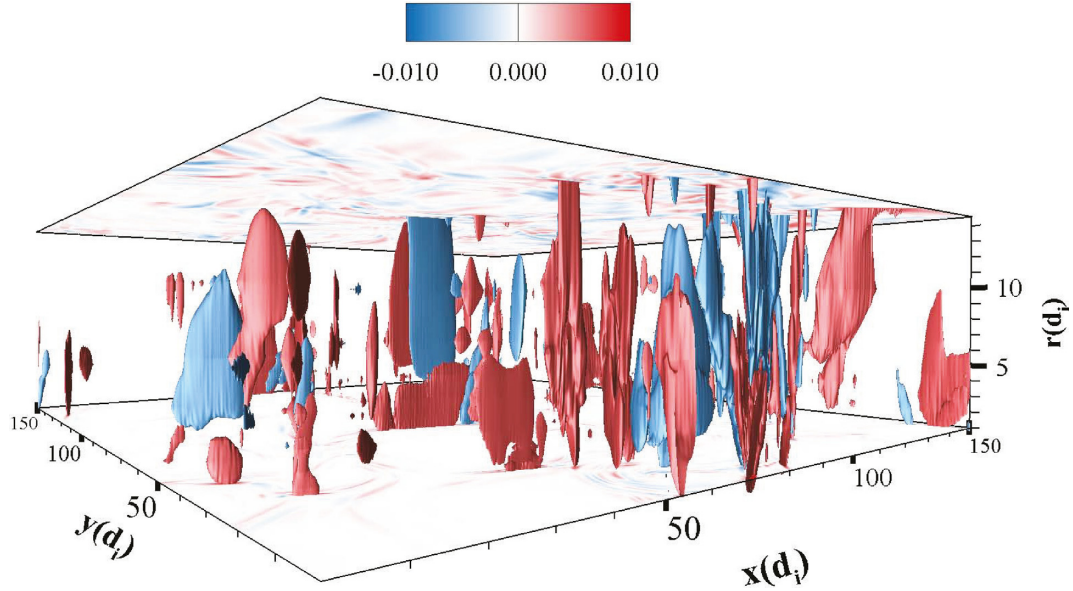
Figure 3. Isosurfaces of the LET in a space spanned by the two spatial dimensions (x, y) and the separation scale r.

contribution to the pressure–strain interaction and the electromagnetic work from different scale bands is $-\left(\boldsymbol{P}_{\alpha}^{[m]} \cdot \nabla\right) \cdot \boldsymbol{u}_{\alpha}^{[n]}$ and $\boldsymbol{j}^{[m]} \cdot \boldsymbol{E}^{[n]}$, respectively.

Fig. 4 shows the normalized contribution to the pressure–strain interaction from different scale bands, $\langle -\left(\boldsymbol{P}_{\alpha}^{[m]} \cdot \nabla\right) \cdot \boldsymbol{u}_{\alpha}^{[n]}\rangle / \langle -\left(\boldsymbol{P}_{\alpha} \cdot \nabla\right) \cdot \boldsymbol{u}_{\alpha}\rangle$, for both electrons and ions. In this paper, the symbol $\langle\rangle$ denotes a volume average over the simulation domain. Remarkably, the band-filtered pressure–strain interaction for electrons densely populates along the diagonal as shown in the plot, as is the case for ions. They are suggestive of a local interaction, namely the interaction mainly involves comparable scales and the contribution from distant bands is negligible. For the normalized contribution to the electromagnetic work from different scale bands, $\langle \boldsymbol{j}^{[m]} \cdot \boldsymbol{E}^{[n]}\rangle / \langle \boldsymbol{j} \cdot \boldsymbol{E}\rangle$ in Fig. 5, notable departures from the diagonal indicate that a wider range of scales are coupled in the interaction. It is beyond the scope of this paper to explore in detail the reasons for which the interactions mainly involve nearby scales, but it may be of some help to refer to the locality of scale interactions in MHD turbulence (Alexakis, Mininni & Pouquet 2005; Verma, Ayyer & Chandra 2005; Aluie & Eyink 2010; Teaca, Carati & Domaradzki 2011; Yang et al. 2016).

Also noteworthy in Fig. 4 is that the most intense (dark blue) contribution to the pressure–strain interaction is confined to a small region very near the origin, i.e. a few d_i. The contribution to the pressure–strain interaction mostly results from small scales, $< 6d_i$ in the present simulation. Note that the full pressure–strain interaction can be further decomposed as $-\left(\boldsymbol{P}_{\alpha} \cdot \nabla\right) \cdot \boldsymbol{u}_{\alpha} = -p_{\alpha}\theta_{\alpha} - \pi_{ij}^{(\alpha)} D_{ij}^{(\alpha)}$, where $\theta_{\alpha} = \nabla \cdot \boldsymbol{u}_{\alpha}$ is the dilatation, $D_{ij}^{(\alpha)} = \left(\partial_i u_j^{(\alpha)} + \partial_j u_i^{(\alpha)}\right)/2 - \theta_{\alpha}\delta_{ij}/3$ is the traceless strain rate tensor, and $\pi_{ij}^{(\alpha)} = P_{ij}^{(\alpha)} - p_{\alpha}\delta_{ij}$ is the deviatoric pressure tensor. The result shown here poses no contradiction with the conclusion in Aluie, Li & Li (2012) and Yang et al. (2016) that the pressure-dilatation derives most of its contribution from large scales, since the pressure-dilatation terms here only account for a small fraction of $\langle -\left(\boldsymbol{P}_{\alpha} \cdot \nabla\right) \cdot \boldsymbol{u}_{\alpha}\rangle$. For example, the global averages of $-\pi_{ij}^{(\alpha)} D_{ij}^{(\alpha)}$, $1.05 \times 10^{-4} \, v_{Ar}^3 d_i^{-1}$ for electrons and $8.57 \times 10^{-5} \, v_{Ar}^3 d_i^{-1}$ for ions

are much greater than those of $-p_{\alpha}\theta_{\alpha}$, $9.03 \times 10^{-6} \, v_{Ar}^3 d_i^{-1}$ for electrons and $-8.14 \times 10^{-6} \, v_{Ar}^3 d_i^{-1}$ for ions. Therefore, the full pressure–strain interaction behaves quite in analogy with the shear associated part $-\pi_{ij}^{(\alpha)} D_{ij}^{(\alpha)}$, which can be cast as viscous dissipation in highly collisional hydrodynamic limit (Braginskii 1965; Vincenti & Kruger 1965). Moving into the realm of strongly compressed plasma, as in the turbulent magnetosheath (Chasapis et al. 2018b), compressibility effect might make a big difference.

The positive contribution to the electromagnetic work in Fig. 5 is concentrated at relatively large scales, $\sim[6d_i, 16d_i]$ in the present simulation. While we make no claims of universality of these scale ranges at which the energy transfer channels dominate, due to differences in accessible parameters in simulations and in direct observational analysis, it does qualitatively support the conjecture that the pressure–strain interaction mainly operates at small scales, while the electromagnetic work acts primarily at relatively large scales.

5 SPATIAL CORRELATION BETWEEN LET AND ENERGY TRANSFER CHANNELS

There is accumulating evidence of the association between coherent structures and plasma dissipation. For example, HVM simulations have shown that strong distortions of the distribution function occur near current sheets (Greco et al. 2012; Servidio et al. 2012). Coherent structures (measured as high 'PVI' events) in any of several variables – density, magnetic field and velocity, are associated with extremal values of proton temperature anisotropy (Servidio et al. 2015). One also finds interesting and inter-related roles of vorticity and symmetric strain in heating (Huba 1996; Del Sarto et al. 2016; Del Sarto & Pegoraro 2017; Franci et al. 2016; Parashar & Matthaeus 2016). Meanwhile, all the energy dissipation proxies discussed above, the local energy transfer rate (LET), the electromagnetic work $\boldsymbol{j} \cdot \boldsymbol{E}$ and the pressure–strain interaction $-\left(\boldsymbol{P} \cdot \nabla\right) \cdot \boldsymbol{u}$, are systematically concentrated in space, and these concentrations occur within or very near coherent structures (Wan et al. 2012, 2016; Parashar & Matthaeus 2016; Yang et al. 2017a,c; Sorriso-Valvo et al. 2018a,b).
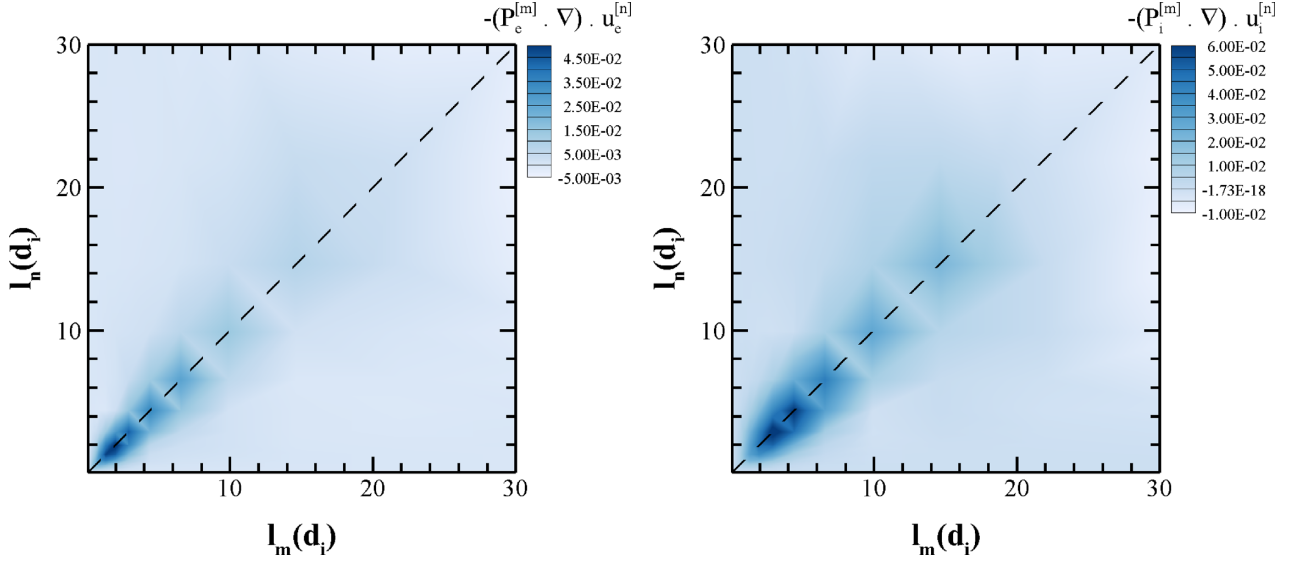
Figure 4. Normalized contribution to the pressure–strain interaction from different scale bands, $\langle -\left(P_\alpha^{[m]} \cdot \nabla\right) \cdot u_\alpha^{[n]}\rangle / \langle -\left(P_\alpha \cdot \nabla\right) \cdot u_\alpha\rangle$, for both (left) electrons and (right) ions.
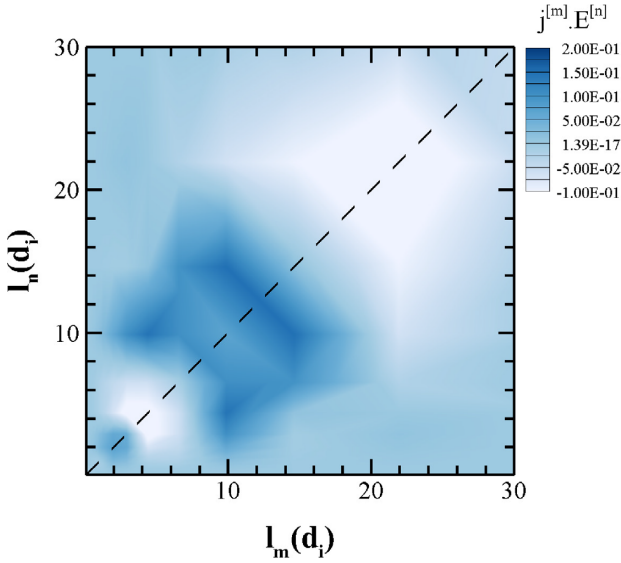

Figure 5. Normalized contribution to the electromagnetic work from different scale bands, $\langle j^{[m]} \cdot E^{[n]}\rangle / \langle j \cdot E\rangle$.

The connection between coherent structures and energy transfer represents yet another way in which coherent structures and intermittency contribute to plasma dissipation and heating, further advancing a complementary view that has been emerging in recent years: energy cascade leads to several channels of energy conversion, interchange and spatial rearrangement that collectively leads to production of internal energy. Given the diversity of energy dissipation proxies that may dominate at different scales, a significant question is the extent to which they are related in the overall picture of intermittent heating.

For a first diagnostic to address these questions, Fig. 6 shows spatial contour maps of the LET at $5d_i$ (i.e. $\epsilon_{r=5d_i}$), $j \cdot E$ and $-(P \cdot \nabla) \cdot u$ separately for protons and electrons in several sub-regions. The first thing to notice is that these energy dissipation

proxies are highly localized with intense values concentrated at small regions. Also seen immediately is the greatly similar pattern of their spatial distributions, though point-wise magnitudes and signs might be different. The striking similarity between the spatial patches of the different proxies suggests that coherent structures, energy transfer and dissipation are all correlated to a certain extent.

We compute the global volume averages of energy dissipation proxies, as shown in Table 1. These entries in the table, wherein $\langle -(P_e \cdot \nabla) \cdot u_e\rangle + \langle -(P_i \cdot \nabla) \cdot u_i\rangle \sim 1.92 \times 10^{-4}\ (v_{Ar}^3 d_i^{-1})$, are meaningfully compared with the mean energy dissipation rate estimated by the third-order law, $\epsilon \sim 1.87 \times 10^{-4}\ (v_{Ar}^3 d_i^{-1})$. It is interesting to note that $\langle j \cdot E\rangle$ is negative, suggesting that kinetic energy of particles is converted into electromagnetic energy at this moment. We found that the global average of the electromagnetic work oscillates significantly over time at high frequencies (comparable to ω_{pe}). This is likely an artefact of the artificial value of ω_{pe}/ω_{ce} in our simulation, and could be remedied by time averaging the results over a plasma oscillation period (Haggerty et al., in preparation). As computed by Wan et al. (2015, 2016), the energy conversion rate in the frame moving with electrons $\langle D_e\rangle = \langle j \cdot (E + u_e \times B) - \rho_c (u_e \cdot E)\rangle$ is somewhat lower than ε and $\langle -(P_e \cdot \nabla) \cdot u_e\rangle + \langle -(P_i \cdot \nabla) \cdot u_i\rangle$. Thus this measure may only account for a part of total dissipation.

More diagnostics, such as scatter plots of any two proxies (not shown here) and the corresponding Spearman correlation coefficients ρ_s, can be used to clarify the possible correlation. However, their Spearman correlation coefficients are rather small, e.g. $\rho_s(\left|\epsilon_{r=5d_i}\right|, |j \cdot E|) = 0.25$, $\rho_s(\left|\epsilon_{r=5d_i}\right|, |-(P_e \cdot \nabla) \cdot u_e|) = 0.042$ and $\rho_s(|j \cdot E|, |-(P_e \cdot \nabla) \cdot u_e|) = 0.057$. The conclusion drawn in this way may seem at first to be in conflict with the finding of Fig. 6. But it is maybe not so surprising that there is not a strong point-wise correlation amongst the LET, the pressure–strain interaction and the electromagnetic work. This recalls the lower correlation between proton heating and current relative to vorticity, and related findings (Servidio et al. 2015; Del Sarto et al. 2016; Franci et al. 2016; Parashar & Matthaeus 2016). According to equations (4)–(6), the transport terms on the left-hand side could be locally enormous, thus spoiling co-location of the proxies.
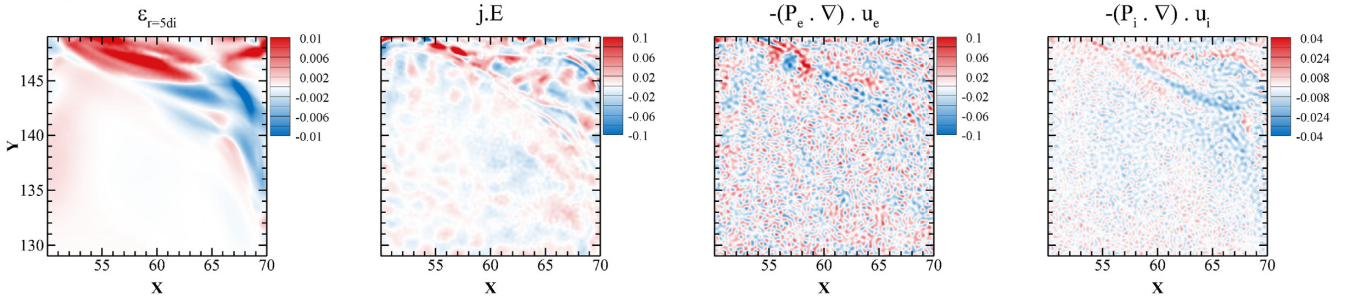
Subregion 1
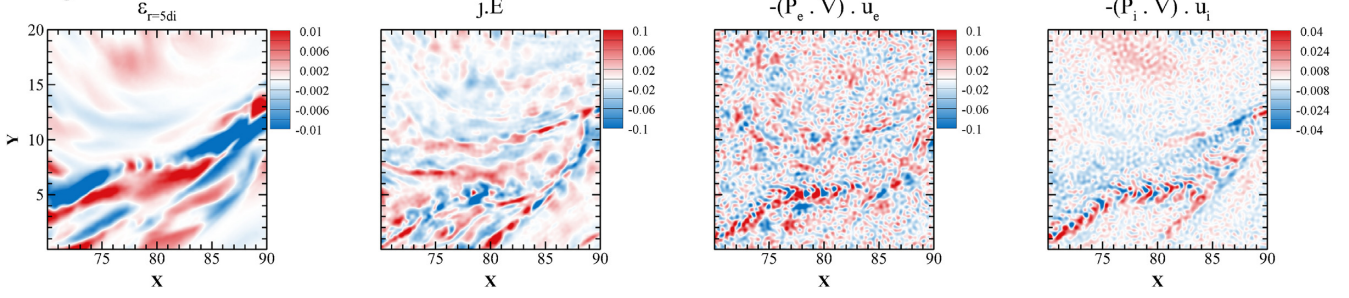
Subregion 2
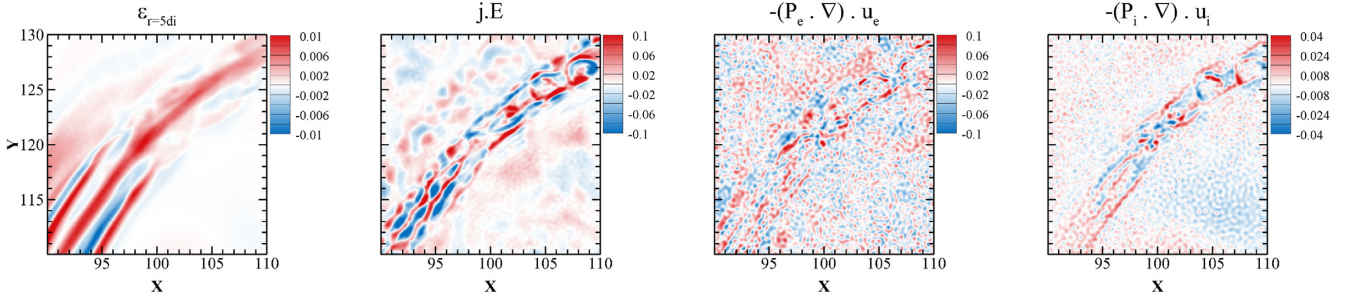
Subregion 3

Figure 6. Contours for $\epsilon_{r=5d_i}$, $\boldsymbol{j} \cdot \boldsymbol{E}$, $-(\boldsymbol{P}_e \cdot \nabla) \cdot \boldsymbol{u}_e$ and $-(\boldsymbol{P}_i \cdot \nabla) \cdot \boldsymbol{u}_i$ at small subregions.

Table 1. Volume averages of the LET, the electromagnetic work, the pressure–strain interaction and the electron-frame dissipation measure D_e (Zenitani et al. 2011). Quantities listed are in the code units $v_{Ar}^3 d_i^{-1}$.

ε^a	$\langle \boldsymbol{j} \cdot \boldsymbol{E} \rangle$	$\langle \boldsymbol{j}_e \cdot \boldsymbol{E} \rangle^b$	$\langle \boldsymbol{j}_i \cdot \boldsymbol{E} \rangle^c$	$\langle -(\boldsymbol{P}_e \cdot \nabla) \cdot \boldsymbol{u}_e \rangle$	$\langle -(\boldsymbol{P}_i \cdot \nabla) \cdot \boldsymbol{u}_i \rangle$	$\langle D_e \rangle^d$
1.87×10^{-4}	-5.1×10^{-5}	1.24×10^{-4}	-1.75×10^{-4}	1.14×10^{-4}	7.8×10^{-5}	1.42×10^{-4}

[a]Volume average of the LET ε_r evaluated within $[2d_i, 10d_i]$ range.
[b,c]Separate contributions of electrons and protons to the electromagnetic work.
[d]The work done by electromagnetic fields on particles, evaluated in the frame of electron bulk motion.

We anticipate then that the energy dissipation proxies in the subsequent energy transfer are juxtaposed to, but not exactly co-located with one another. This complex spatial arrangement can best be illustrated by a scale-dependent cross-correlation function,

$$R(f, g, r) = \frac{\langle (f(\boldsymbol{x} + \boldsymbol{r}) - \langle f \rangle)(g(\boldsymbol{x}) - \langle g \rangle) \rangle}{\langle (f(\boldsymbol{x}) - \langle f \rangle)(g(\boldsymbol{x}) - \langle g \rangle) \rangle}, \quad (9)$$

where f and g are the fields and the direction of displacement $\boldsymbol{r}$ is arbitrary for isotropic turbulence in the plane. Such correlations have been used to show strong correlations between hotter plasma and vorticity as compared to the correlations between hotter plasma and current (Parashar & Matthaeus 2016), although the correlations

were not normalized in the same fashion there. Seen in Fig. 7 is that the correlation curves peak near $2d_i$. It is natural that the statistical connection between the proxies will become infinitely attenuated as the points become infinitely far apart in space. (This follows from the familiar clustering property of turbulent fluctuations.) It is then possible to calculate a correlation length, $\lambda_c(f, g) = \int_0^\infty R(f, g, r) dr$, a convenient measure of the spatial extent over which the fields are appreciably correlated. The results are shown in Table 2. There is clear delocalization between the proxies, so that $-(\boldsymbol{P}_\alpha \cdot \nabla) \cdot \boldsymbol{u}_\alpha$ and $\boldsymbol{j} \cdot \boldsymbol{E}$ are larger near, not necessarily at, locations of large $\epsilon_{r=5d_i}$. Note that the short correlation length associated with $\boldsymbol{j} \cdot \boldsymbol{E}$ is in part due to its reversal of sign around spatial separation $r = 4d_i$.
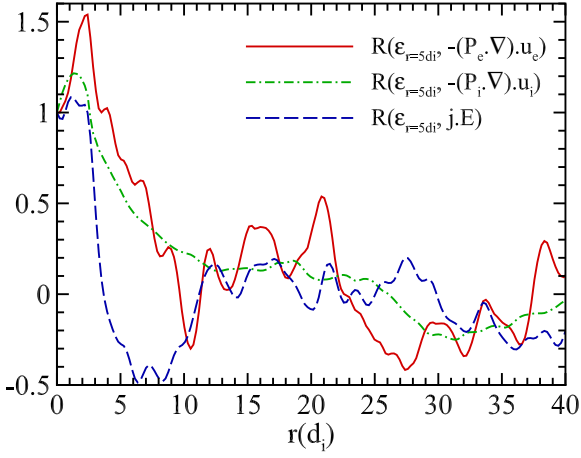
Figure 7. Two-point cross-correlation functions of $\epsilon_{r=5d_i}$, $\boldsymbol{j} \cdot \boldsymbol{E}$, $-(\boldsymbol{P}_e \cdot \nabla) \cdot \boldsymbol{u}_e$ and $-(\boldsymbol{P}_i \cdot \nabla) \cdot \boldsymbol{u}_i$.

Table 2. Correlation lengths estimated from the data in Fig. 7.

Proxies	λ_c (d_i)
$\left(\epsilon_{r=5d_i}, -(\boldsymbol{P}_e \cdot \nabla) \cdot \boldsymbol{u}_e\right)$	7.85
$\left(\epsilon_{r=5d_i}, -(\boldsymbol{P}_i \cdot \nabla) \cdot \boldsymbol{u}_i\right)$	4.72
$\left(\epsilon_{r=5d_i}, \boldsymbol{j} \cdot \boldsymbol{E}\right)$	1.77

6 CONCLUSIONS

The dissipative mechanism in weakly collisional plasma is a topic that pervades decades of studies without a consensus solution. One popular approach to explain dissipation is to resort to wave particle interactions, with instabilities regulating the dynamics of extreme distortions of the distribution function. A complementary view is that several channels of energy conversion emerge in a turbulence cascade process. In this paper, we study energy dissipation proxies based on the cascade, i.e. the local energy transfer rate (LET), the electromagnetic work $\boldsymbol{j} \cdot \boldsymbol{E}$ and the pressure–strain interaction $-(\boldsymbol{P}_\alpha \cdot \nabla) \cdot \boldsymbol{u}_\alpha$.

We find that although these proxies are displaced in space, enhanced electromagnetic work and pressure–strain interaction are concentrated in the proximity of regions with intense LET. Their connection is a somewhat atypical property in that it is not readily found using point-wise correlation, but rather one must appeal to statistics, such as two-point cross-correlation functions, to understand it. The basis for their association but also delocalization in space lies in a recognition of the key steps of energy transfer: conservative rearrangement of energy in space due to transport terms; conservative rearrangement of energy in scales due to energy cascade; electromagnetic work on particles that drives flows; and pressure–strain interactions that produce internal energy.

The association between the LET and energy transfer channels in this paper, in conjunction with the results in Hall MHD (Camporeale et al. 2018) and compressible MHD (Yang et al. 2016, 2017b), should be an adequate starting point for further investigating, for example, how do the characteristics of energy transfer vary going from MHD to kinetic scales. We show here that there is a decade of range, $\sim[2d_i, 10d_i]$, over which the third-order law is valid. It is also found that contributions to $\boldsymbol{j} \cdot \boldsymbol{E}$ and $-(\boldsymbol{P}_\alpha \cdot \nabla) \cdot \boldsymbol{u}_\alpha$ are

mainly from large ($\sim[6d_i, 16d_i]$ in this simulation) and small ($<6d_i$ in this simulation) scales, respectively. Therefore, these proxies are dominated at different scales.

Taken together, their connections and differences further support this intuitive picture (Yang et al. 2017c): the cascade drives scale-to-scale energy transfer, with a net transfer of energy to small scales, and leads to intermittent distributions of several channels of energy conversion that in turn provide the dominate dissipation mechanism. Electromagnetic energy is converted into flows by electromagnetic work, while pressure–strain interaction converts energy from flows into internal energy. Note that none of the three dissipation proxies we examined are sign-definite, and therefore some type of averaging is necessary to interpret any of them as a net rate of conversion or transfer in the complex pathways to dissipation and heating. It is worth emphasizing that our 2.5D PIC simulation is not intended to reproduce any particular solar wind feature or data interval. While this model is a powerful tool, it also fails to properly account for important real effects, such as solar wind expansion, three dimensionality, ion-to-electron mass ratio, and so on. Consequently, a report such as the present one necessarily leads to an incomplete description of energy dissipation. We anticipate our results to be extended to more sophisticated models in future works.

REFERENCES

Alexakis A., Mininni P. D., Pouquet A., 2005, Phys. Rev. E, 72, 046301
Aluie H., Eyink G. L., 2010, Phys. Rev. Lett., 104, 081101
Aluie H., Li S., Li H., 2012, ApJ, 751, L29
Andrés N., Galtier S., Sahraoui F., 2018, Phys. Rev. E, 97, 013204
Bale S. D., Kellogg P. J., Mozer F. S., Horbury T. S., Reme H., 2005, Phys. Rev. Lett., 94, 215002
Bandyopadhyay R. et al., 2018a, ApJ, 866, 81
Bandyopadhyay R. et al., 2018b, ApJ, 866, 106
Banerjee S., Galtier S., 2013, Phys. Rev. E, 87, 013019
Banerjee S., Hadid L. Z., Sahraoui F., Galtier S., 2016, ApJ, 829, L27
Braginskii S. I., 1965, Rev. Plasma Phys., 1, 205
Camporeale E., Sorriso-Valvo L., Califano F., Retinò A., 2018, Phys. Rev. Lett., 120, 125101
Carbone V., Marino R., Sorriso-Valvo L., Noullez A., Bruno R., 2009, Phys. Rev. Lett., 103, 061102
Chasapis A. et al., 2018a, ApJ, 856, L19
Chasapis A. et al., 2018b, ApJL, 862, 32
Coburn J. T., Forman M. A., Smith C. W., Vasquez B. J., Stawarz J. E., 2015, Phil. Trans. R. Soc. A, 373, 20140150
Del Sarto D., Pegoraro F., Califano F., 2016, Phys. Rev. E, 93, 053203
Del Sarto D., Pegoraro F., 2017, MNRAS, 475, 181
Dmitruk P., Matthaeus W. H., Seenu N., 2004, ApJ, 617, 667
Ergun R. et al., 2018, Geophys. Res. Lett., 45, 3338
Forman M. A., Smith C. W., Vasquez B. J., 2010, Phys. Rev. Lett., 104, 189001

Franci L., Hellinger P., Matteini L., Verdini A., Landi S., 2016, in AIP Conf. Ser. Vol. 1720, Solar Wind 14: Fourteenth International Solar Wind Conference. Am. Inst. Phys., San Francisco, p. 040003

Fu H., Vaivads A., Khotyaintsev Y. V., André M., Cao J., Olshevsky V., Eastwood J., Retino A., 2017, Geophys. Res. Lett., 44, 37

Galtier S., 2008, Phys. Rev. E, 77, 015302

Gary S. P., Saito S., 2003, J. Geophys. Res., 108, 1194

Gary S. P., Saito S., Li H., 2008, Geophys. Res. Lett., 35, L02104

Germano M., 1992, J. Fluid Mech., 238, 325

Gogoberidze G., Perri S., Carbone V., 2013, ApJ, 769, 111

Goldreich P., Sridhar S., 1995, ApJ, 438, 763

Greco A., Valentini F., Servidio S., Matthaeus W. H., 2012, Phys. Rev. E, 86, 066405

Hadid L., Sahraoui F., Galtier S., 2017, ApJ, 838, 9

He J., Wang L., Tu C., Marsch E., Zong Q., 2015a, ApJ, 800, L31

He J. et al., 2015b, ApJ, 813, L30

He J. et al., 2018, ApJ, 856, 148

Hellinger P., Trávníček P. M., Štverák Š., Matteini L., Velli M., 2013, J. Geophys. Res.: Space Phys., 118, 1351

Hellinger P., Verdini A., Landi S., Franci L., Matteini L., 2018, ApJ, 857, L19

Hollweg J. V., 1986, J. Geophys. Res., 91, 4111

Hollweg J. V., Isenberg P. A., 2002, J. Geophys. Res., 107, 1147

Howes G., Dorland W., Cowley S., Hammett G., Quataert E., Schekochihin A., Tatsuno T., 2008, Phys. Rev. Lett., 100, 065004

Howes G. G., McCubbin A. J., Klein K. G., 2018, J. Plasma Phys., 84, 905840105

Howes G. G., TenBarge J. M., Dorland W., Quataert E., Schekochihin A. A., Numata R., Tatsuno T., 2011, Phys. Rev. Lett., 107, 035004

Huba J. D., 1996, Geophys. Res. Lett., 23, 2907

Kritsuk A. G., Ustyugov S. D., Norman M. K., Padoan P., 2009, J. Phys. Conf. Ser., 180, 012020

MacBride B. T., Smith C. W., 2008, ApJ, 679, 1644

Marino R., Sorriso-Valvo L., Carbone V., Veltri P., Noullez A., Bruno R., 2011, Planet. Space Sci., 59, 592

Marino R., Sorriso-Valvo L., Carbone V., Noullez A., Bruno R., Bavassano B., 2008, ApJ, 677, L71

Markovskii S. A., Vasquez B. J., Smith C. W., Hollweg J. V., 2006, ApJ, 639, 1177

Marsch E., Tu C.-Y., 1997, Nonlinear Processes Geophys., 4, 101

Narita Y., Gary S. P., Saito S., Glassmeier K., Motschmann U., 2011, Geophys. Res. Lett., 38, 387

Osman K., Kiyani K., Matthaeus W., Hnat B., Chapman S., Khotyaintsev Y. V., 2015, ApJ, 815, L24

Osman K. T., Matthaeus W. H., Greco A., Servidio S., 2011, ApJ, 727, L11

Parashar T. N., Matthaeus W. H., 2016, ApJ, 832, 57

Parashar T. N., Matthaeus W. H., Shay M. A., 2018, ApJL, 864, L21

Parashar T. N., Servidio S., Shay M. A., Breech B., Matthaeus W. H., 2011, Phys. Plasmas, 18, 092302

Perri S., Goldstein M. L., Dorelli J. C., Sahraoui F., 2012, Phys. Rev. Lett., 109, 191101

Podesta J., 2008, J. Fluid Mech., 609, 171

Politano H., Pouquet A., 1998, Phys. Rev. E, 57, R21

Retinò A., Sundkvist D., Vaivads A., Mozer F., André M., Owen C. J., 2007, Nat. Phys., 3, 235

Sahraoui F., Goldstein M. L., Belmont G., Canu P., Rezeau L., 2010, Phys. Rev. Lett., 105, 131101

Sahraoui F., Goldstein M. L., Robert P., Khotyaintsev Y. V., 2009, Phys. Rev. Lett., 102, 231102

Saito S., Gary S. P., Li H., Narita Y., 2008, Phys. Plasmas, 15, 102305

Schekochihin A., Cowley S., Dorland W., Hammett G., Howes G., Plunk G., Quataert E., Tatsuno T., 2008, Plasma Phys. Control. Fusion, 50, 124024

Servidio S., Valentini F., Califano F., Veltri P., 2012, Phys. Rev. Lett., 108, 045001

Servidio S., Valentini F., Perrone D., Greco A., Califano F., Matthaeus W. H., Veltri P., 2015, J. Plasma Phys., 81, 325810107

Sitnov M., Merkin V., Roytershteyn V., Swisdak M., 2018, Geophys. Res. Lett., 45, 4639

Smith C. W., Vasquez B. J., Hollweg J. V., 2012, ApJ, 745, 8

Sorriso-Valvo L., Carbone F., Perri S., Greco A., Marino R., Bruno R., 2018b, Solar Phys., 293, 10

Sorriso-Valvo L., Carbone V., Marino R., Noullez A., Bruno R., Veltri P., 2010, Phys. Rev. Lett., 104, 189002

Sorriso-Valvo L., Carbone V., Noullez A., Politano H., Pouquet A., Veltri P., 2002, Phys. Plasmas, 9, 89

Sorriso-Valvo L., Perrone D., Pezzi O., Valentini F., Servidio S., Zouganelis I., Veltri P., 2018a, J. Plasma Phys., 84, 725840201

Sorriso-Valvo L. et al., 2007, Phys. Rev. Lett., 99, 115001

Stawarz J. E., Smith C. W., Vasquez B. J., Forman M. A., MacBride B. T., 2009, ApJ, 697, 1119

Stawarz J. E., Vasquez B. J., Smith C. W., Forman M. A., Klewicki J., 2011, ApJ, 736, 44

Sundkvist D., Retinò A., Vaivads A., Bale S. D., 2007, Phys. Rev. Lett., 99, 025004

Teaca B., Carati D., Domaradzki J. A., 2011, Phys. Plasmas, 18, 112307

TenBarge J. M., Howes G. G., 2013, ApJ, 771, L27

Verma M. K., Ayyer A., Chandra A. V., 2005, Phys. Plasmas, 12, 082307

Vincenti W. G., Kruger C. H., 1965, Introduction to Physical Gas Dynamics, Wiley, New York

Wan M., Matthaeus W. H., Roytershteyn V., Karimabadi H., Parashar T., Wu P., Shay M., 2015, Phys. Rev. Lett., 114, 175002

Wan M., Matthaeus W. H., Roytershteyn V., Parashar T. N., Wu P., Karimabadi H., 2016, Phys. Plasmas, 23, 042307

Wan M., Servidio S., Oughton S., Matthaeus W. H., 2009, Phys. Plasmas, 16, 090703

Wan M., Servidio S., Oughton S., Matthaeus W. H., 2010, Phys. Plasmas, 17, 052307

Wan M. et al., 2012, Phys. Rev. Lett., 109, 195001

Yang Y., Matthaeus W. H., Shi Y., Wan M., Chen S., 2017b, Phys. Fluid, 29, 035105

Yang Y., Shi Y., Wan M., Matthaeus W. H., Chen S., 2016, Phys. Rev. E, 93, 061102

Yang Y. et al., 2017a, Phys. Plasmas, 24, 072306

Yang Y. et al., 2017c, Phys. Rev. E, 95, 061201

Yao Z. et al., 2017, J. Geophys. Res.: Space Phys., 122, 4335

Zeiler A., Biskamp D., Drake J. F., Rogers B. N., Shay M. A., Scholer M., 2002, J. Geophys. Res., 107, 1230

Zenitani S., Hesse M., Klimas A., Kuznetsova M., 2011, Phys. Rev. Lett., 106, 195003

This paper has been typeset from a TEX/LATEX file prepared by the author.